^{1}H AND ^{15}N NMR Sequential Assignment, Secondary Structure, and Tertiary Fold of [2Fe-2S] Ferredoxin from *Synechocystis* sp. PCC 6803†

Cécile Lelong,‡,§ Pierre Sétif,*,‡,§ Hervé Bottin,‡,§ François André,‡ and Jean-Michel Neumann*,§,||

CEA, Département de Biologie Cellulaire et Moléculaire, Section de Bioénergétique, Section de Biophysique des Protéines Membranaires and CNRS URA 1290, C. E. Saclay, 91191 Gif sur Yvette Cedex, France

Received July 10, 1995; Revised Manuscript Received September 5, 1995⊗

ABSTRACT: The [2Fe-2S] ferredoxin extracted from *Synechocystis* sp. PCC 6803 was studied by ^{1}H and ^{15}N nuclear magnetic resonance. Sequence-specific ^{1}H and ^{15}N assignment of amino acid residues far from the paramagnetic cluster (distance higher than 8 Å) was performed. Interresidue NOE constraints have allowed the identification of several secondary structure elements: one β sheet composed of four β strands, one α helix, and two α helix turns. The analysis of interresidue NOEs suggests the existence of a disulfide bridge between the cysteine residues 18 and 85. Such a disulfide bridge has never been observed in plant-type ferredoxins. Structure modeling using the X-PLOR program was performed with or without assuming the existence of a disulfide bridge. As a result, two structure families were obtained with rms deviations of 2.2 Å. Due to the lack of NOE connectivities resulting from the paramagnetic effect from the [2Fe-2S] cluster, the structures were not well resolved in the region surrounding the [2Fe-2S] cluster, at both extremities of the α helix and the C and N terminus segments. In contrast, when taken separately, the β sheet and the α helix were well defined. This work is the first report of a structure model of a plant-type [2Fe-2S] Fd in solution.

The [2Fe-2S] chloroplast-type ferredoxins are distributed in various oxygenic photosynthetic organisms. They are small proteins, having a molecular mass of about 11 kDa and strongly acidic with highly homologous amino acid sequences (Rogers, 1987; Matsubara & Wada, 1988; Knaff & Hirasawa, 1991). They function as an electron donor in many metabolic pathways (Knaff & Hirasawa, 1991) whereas most of them function as an electron acceptor to photosystem I. Four different structures of cyanobacterial ferredoxins (Tsukihara et al., 1981, 1990; Rypniewski et al., 1991; Jacobson et al., 1993) as well as one from horsetail (Ikemizu et al., 1994) have been determined by X-ray crystallography at high resolution. All of them are very similar with the highest structural homology around the paramagnetic cluster and a high proportion of β sheet in the diamagnetic part of the protein. [2Fe-2S] ferredoxins have also been found in bacteria, vertebrate mitochondria, and oxygenase systems (Matsubara & Saeki, 1992).

Despite their small size, the structures of ferredoxins are difficult to determine by NMR[1] due to the presence of the iron-sulfur cluster, which is paramagnetic at room temperature in any redox state (Fe^{2+}/Fe^{3+} or Fe^{3+}/Fe^{3+} for a [2Fe-2S] cluster). For the nuclei surrounding the cluster, this paramagnetism gives rise to "hyperfine" shifted resonances and to line broadening due to shortened relaxation times. Many NMR studies have been performed on the chloroplast-type ferredoxins: the earlier studies concerned the observation of hyperfine-shifted ^{1}H resonances (Poe et al., 1971; Salmeen & Palmer, 1972; Nagayama et al., 1983; Chan & Markley, 1983e; Bertini et al., 1993). Subsequently, the amino acid residues surrounding the [2Fe-2S] cluster have been studied in the reduced form of ferredoxin from the cyanobacteria *Spirulina platensis* and *Anabaena* and from the red alga *Porphyra umbilicalis* (Dugad & La Mar, 1990; Skjeldal et al., 1991). Recently, with the help of specific ^{15}N labeling, the assignment of amino acids surrounding the paramagnetic cluster has been performed on the heterocyst [2Fe-2S] Fd from *Anabaena* 7120 (Chae & Markley, 1995).

Concurrently with the study of the environment of the paramagnetic cluster, the ^{1}H and ^{13}C resonances from two histidine and four tyrosine residues of *Anabaena variabilis* ferredoxin I were assigned (Chan & Markley, 1983a−d; Chan et al., 1983). The interactions with redox partners have also been studied (Chan & Markley, 1983d). Almost complete sequence-specific ^{13}C, ^{15}N, and ^{1}H resonance assignments of the [2Fe-2S] vegetative and heterocyst ferredoxins from *Anabaena* 7120 were performed by Oh and co-workers (Oh & Markley, 1990a,b; Oh et al., 1990) and Chae et al. (1994), respectively. The identified secondary structure elements of the vegetative [2Fe-2S] Fd (Oh & Markley, 1990a,b) were in accordance with those found in the X-ray structure of the homologous Fd from *S. platensis* (Tsukihara et al., 1981). However, no solution structure has been modeled neither for the vegetative nor for the heterocyst [2Fe-2S] Fd. ^{1}H NMR has also been utilized to investigate [2Fe-2S] proteins from other sources. Extensive sequential ^{1}H resonance assignment and description of the secondary structure elements of oxidized putidaredoxin (Pdx) have also been reported (Pochapsky & Ye, 1991; Ye et al., 1992). A solution structure of Pdx has been recently proposed using

† Atomic coordinates and molecular restraints are available from Brookhaven Protein Data Bank under entry codes 1DOX and 1DOX-mr, respectively.

* To whom correspondence should be addressed.

‡ CEA, Section de Bioénergétique.

§ CNRS URA 1290.

|| CEA, Section de Biophysique des Protéines Membranaires.

⊗ Abstract published in *Advance ACS Abstracts,* October 15, 1995.

[1] Abbreviations: 2D, two dimensional; 3D, three dimensional; COSY, correlated spectroscopy; CPMG, Carr−Purcell−Meiboom−Gill; DQF, double-quantum filtered; Fd, ferredoxin; HMQC, heteronuclear multiple-quantum correlation; HSQC, heteronuclear single-quantum correlation; M_r, molecular mass; NOE, nuclear Overhauser effect; NOESY, two-dimensional NOE spectroscopy; NMR, nuclear magnetic resonance; Pdx, putidaredoxin; rms, root mean square; *Syn.* 6803, *Synechocystis* sp. PCC 6803; T_2, transverse relaxation time; TOCSY, total correlation spectroscopy; TPPI, time-proportional phase incrementation.

0006-2960/95/0434-14462$09.00/0

NOE cross-peaks for the diamagnetic part of the protein and assuming high structural similarities among all [2Fe-2S] clusters and their immediate environment (Pochapsky et al., 1994). The Pdx was the first mammalian-type [2Fe-2S] Fd structurally characterized in solution.

The ferredoxin of *Synechocystis* sp. PCC 6803 has been characterized and sequenced (96 amino acids including six cysteine residues) (Bottin & Lagoutte, 1992). Among the six cysteine residues, four are involved in the [2Fe-2S] cluster binding; the two others were not detected as free thiols, suggesting the presence of a disulfide bridge. This is consistent with the electrophoretic mobility properties, which are largely modified in conditions appropriate for reducing a disulfide bridge (apparent M_r from 2.5 to 16.5 kDa) (Creighton, 1989). The preceding observations, concerning the putative disulfide bridge, stimulated the study of the solution structure of the *Syn.* 6803 ferredoxin by NMR. We first report the signal assignment of the diamagnetic part of the protein from homo- and heteronuclear spectra. Characteristic NOE cross-peaks allowed us to identify most of the secondary structure of ferredoxin. Several differences between secondary structure elements observed in the other chloroplast-type ferredoxins and those observed in *Syn.* 6803 ferredoxin will be described and discussed. The tertiary fold of the *Syn.* 6803 ferredoxin was determined using NMR data and structure modeling performed with or without the assumption of the presence of a disulfide bridge between the cysteine residues 18 and 85. The structure families resulting from both calculations are described. A solution structure model of *Synechocystis* 6803 ferredoxin is proposed.

MATERIALS AND METHODS

Protein Purification. Ferredoxin was isolated from *Synechocystis* sp. PCC 6803 following the method of Ho et al. (1979) and Bottin and Lagoutte (1992), modified as described below. The cyanobacterium *Synechocystis* sp. PCC 6803 was grown autophototrophically in 18 L batch cultures on BG-11 medium (Rippka et al., 1979) (with a 2-fold increased ferric ion concentration). Cells were collected at late logarithmic phase by continuous centrifugation. Pellets were washed once in 10 mM NaCl, 50 mM Tricine, pH 7.8, 1 mM EDTA, and 1 mM of the following protease inhibitors: phenylmethanesulfonyl fluoride, ϵ-amino-*n*-caproic acid, and benzamidine. Cells were resuspended in the same buffer containing DNAse. The suspension was passed four times through a French pressure cell at 20000 lb/in^2. The homogenate was centrifuged for 10 min at 10000*g* and the resulting supernatant centrifuged for 1 h at 200000*g* to sediment the thylakoid membranes. The resulting supernatant containing soluble proteins was successively brought to 45, 55, 70, 90, and 100% saturated $(NH_4)_2SO_4$. The 100% saturated $(NH_4)_2SO_4$ supernatant was loaded onto a DEAE-cellulose column (DE 52, Whatman) equilibrated with saturated $(NH_4)_2SO_4$. The column was first washed with two volumes of saturated $(NH_4)_2SO_4$, and then two volumes of distilled water and eluted with 2 M NaCl. The red eluate was then concentrated and rinsed several times by ultrafiltration (Centriprep 10, Amicon) with 20 mM Tricine/NaOH, pH 7.8, containing 0.04 mg/mL ribonuclease A. The concentrated extract was then loaded onto an hydrophobic chromatography column (Octyl-Sepharose CL-4B, Pharmacia) equilibrated with saturated $(NH_4)_2SO_4$. The Fd was eluted using a linear $(NH_4)_2SO_4$ gradient (100−0%). The eluted ferredoxin was again dialyzed by ultrafiltration (Centriprep 10) with 20 mM Tricine/NaOH, pH 7.8, in the presence of ribonuclease A. Final purification was achieved by FPLC chromatography on an anion exchanger column (Mono Q HR5/5, Pharmacia) equilibrated with 20 mM Tricine/NaOH, pH 7.8, and the Fd was eluted by a linear NaCl gradient (0−1 M). At each step, the A_{422}/A_{276} and A_{330}/A_{276} ratios were measured. Ferredoxin solutions were considered to be pure when these ratios were equal or higher than 0.52 and 0.68, respectively.

Uniformely ^{15}N-labeled ferredoxin was produced by growing the cyanobacterium *Synechocystis* sp. PCC 6803 on the same medium as above containing sodium (^{15}N) nitrate (99% atom ^{15}N, Euriso-top, CEA Group) as the sole nitrogen source.

Samples Preparation. NMR samples contained generally 5−9 mM ferredoxin in 0.5 mL of 100 mM phosphate buffer at pH 4.5−6.5, containing 10% (v/v) D_2O. In some samples, 100 mM NaCl was added. Fd samples in H_2O were prepared by ultrafiltration (Centriprep 10) in the phosphate buffer and concentrated to 0.5 mL. The sample in D_2O was prepared in the same way with 100 mM phosphate buffer (pH 6.5) previously lyophilized and redissolved in D_2O (99.8% atom ^2H). The procedure was repeated three times. Another procedure was used for the ^{15}N-labeled Fd: Fd was washed with H_2O by ultrafiltration (Centricon 10), lyophilized, and then dissolved in 0.5 mL of D_2O (99.8% atom ^2H). The sample was lyophilized once again and then was dissolved in 0.5 mL of 100 mM phosphate buffer, 100 mM NaCl, and 1 mM EDTA which was previously twice lyophilized and dissolved in D_2O.

NMR Experiments: Samples in H_2O/D_2O (90:10) Solutions. ^1H NMR data were obtained using a Bruker AMX-600 spectrometer at different temperatures from 10 to 37 °C and different pH values from 4.5 to 6.5. All the data were processed and analyzed using the Bruker UXNMR software. TPPI was used to obtain phase-sensitive DQF-COSY, TOCSY, and NOESY experiments. Mixing times were 80 and 100 ms for the TOCSY and NOESY experiments, respectively. Water suppression was achieved by either presaturation or "jump and return" pulse sequence (Plateau & Guéron, 1982). In some cases, a combination of both water suppression methods was used. In general, a total of 64 or 80 transients was acquired with a recycling delay of 1 s and a spectral width of 7.2 kHz. Four hundred increments of 2K data points were collected in each 2D experiment. Shifted squared sine-bell functions were used for apodization. $^1H-^{15}N$ heteronuclear NMR data were acquired on a Bruker AMX-500 at 15 and 20 °C at pH 5.0. 2D HMQC, HSQC, HMQC-COSY (Gronenborn et al., 1989), HSQC-TOCSY, and HSQC-NOESY (Lerner & Bax, 1986) phase-sensitive experiments were performed using mixing times of 80 ms (TOCSY) and 100 ms (NOESY). A presaturation pulse was used for water suppression and the GARP decoupling scheme (Shaka et al., 1985) was applied to the ^{15}N spins during detection. Eighty transients were acquired with a recycling delay of 1 s and spectral widths of 6 (^1H) and 2.4 kHz (^{15}N). Four hundred increments of 2K data points were collected for each 2D homo- and heteronuclear experiment. Shifted sine-bell functions were used for apodization.

Samples in D_2O Solutions. The same homonuclear and heteronuclear experiments were performed with the D_2O sample. Experimental conditions were also the same except that only two temperatures (10 and 20 °C) and one pH value (6.2) were used. In addition to the set of heteronuclear

experiments described above, ^{15}N transverse relaxation measurements were performed at 20 °C using the two-dimensional experimental scheme given by Kay et al. (1989). Experimental conditions were those mentioned above for the heteronuclear experiments except for the recycling delay increased to 2 s. The CPMG refocusing delay was 1 ms.

Modeling of the Iron−Sulfur Cluster and Its Surroundings. For modeling the iron−sulfur cluster and its surroundings, we followed the approach used by Pochapsky et al. (1994) for Pdx. This approach was successful despite the low sequence homology between Pdx and chloroplast type Fds. A fortiori, this approach is suitable to all the chloroplast-type Fds since they exhibit high sequence homology and structural similarity. In this paper, the cluster and its surroundings were modeled assuming a structural homology between all the types of [2Fe-2S] Fds.

Cluster Modeling. The bond lengths and angle between the iron and inorganic sulfur atoms of the cluster were obtained from the four molecules in the crystal unit of *Aphanothece sacrum* Fd structure (Tsukihara et al., 1990). Average values of the distances and dihedral angles between the ligating cysteines and the cluster (Table 1, Supporting Information)) were imposed to generate the "initial structure" (see *Structural Calculations*). The average values of dihedral angles and distances used to model the residues surrounding the iron−sulfur cluster (Table 2, Supporting Information) were obtained from *A. sacrum* Fd structure. They were imposed as NOE constraints and were subjected to the same violations penalties as other covalent bonds.

Constraints Based on Paramagnetic Broadening Patterns. Oh and Markley (1990a) observed that protons closer than 8 Å to the [2Fe-2S] cluster were not observed on 2D NMR spectra in *Anabaena* Fd by comparison with the X-ray structure. Phe 23−Leu 25, Leu 35−Gly 49, Gln 61−Asp 66, and Val 74−Ala 79 segments were not observed in the 2D spectra. The cross-peaks observed for Leu 25, Leu 35, Gly 49, Val 74, and Ala 79 residues were broadened. We measured the interproton distances $H_\alpha(i)$/Fe and $H_\alpha(i)$/S for the corresponding residues of *A. sacrum* Fd [from the X-ray structure (Tsukihara et al., 1990)]. These distances were found to range from 3 to 11 Å. Based on the high structural conservation observed for the residues surrounding the iron−sulfur cluster, these distances for the above residues of *Syn.* 6803 Fd were constrained to a distance ranging from 3 to 11 Å during the calculations. Similarly, the H_α protons of residues not affected by the paramagnetic cluster were constrained to be distant from the iron−sulfur cluster at distances ranging from 9.0 to 30.0 Å. These computational conditions were applied to the residues belonging to the peptide segments Ala 1−Thr 22, Ala 27−Leu 33, Thr 52−Ser 59, Gln 68−Gly 72, and Pro 81−Tyr 96. These constraints were imposed as NOE constraints in the calculations.

NOE Constraints. A total of 831 distance constraints were used. These included 178 cluster-based distance constraints derived from the paramagnetic broadening effects (52 distances to the cluster of less than 11 Å, and 126 distances to the cluster of more than 9 Å), 191 intraresidue constraints, 210 sequential constraints, 67 medium-range constraints [composed of 37 (i,i+2), 21 (i,i+3), and 9 (i,i+4)], 137 long-range constraints, 6 constraints between the Cα of the cysteine residues ligating the [2Fe-2S] cluster (Table 2, Supporting Information), and 42 constraints defining 21 hydrogen bonds (7 hydrogen bonds in a helical region and 14 in the β sheet). The hydrogen bond constraints were derived from analysis of amide proton exchange rates and included in the calculations only in the refinement steps, after the simulated annealing calculations provided unambiguous identification of the hydrogen bond acceptor. Inter- and intraresidue NOEs were derived from the 100 ms homonuclear NOESY spectrum and converted into an interproton distance by normalizing their integrated cross-peak volume against a calibrated volume. For the calibration, the average volume of 20 resolved $H_{\beta1}-H_{\beta2}$ cross-peaks was used to calculate a reference distance. The cross-peaks were classified as strong, medium, weak, or very weak on the basis of an interproton distance ranging between 1.8 Å and 2.7, 3.5, 5.0, and 6.0 Å, respectively. Multiple atom selections have been used for unresolved NOE cross-peaks, i.e., those of methyl groups, aromatic equivalent protons, and prochiral centers, using the pseudoatom corrections to the distance ranges suggested by Wüthrich (1986). A total of 37 constraints on the backbone torsion angles were used. Thirty torsion angle constraints were derived from the iron−sulfur cluster constraints (see above). The seven remaining constraints (φ torsion angles) were derived from the accessible values of $^3J_{H\alpha N}$ coupling constants measured in a high-resolution HMQC spectrum.

Structural Calculations. Three-dimensional structures calculations were performed using the X-PLOR software package (version 3.0, 1992, Axel T. Brünger) on a Silicon Graphics Indy R4400 workstation. The initial structure was generated using a set of coordinates obtained from the X-ray structure of *A. sacrum* Fd (Tsukihara et al., 1990). One template coordinate set was generated to provide the starting point for the ab initio simulated annealing protocol. This template structure is a stretched conformation. The protocol included the appropriate connectivities and parameters required for the $Fe_2S_2Cys_4$ cluster. The nonbonded energy components during the Verlet dynamics were purely repulsive (repel function), with a short cutoff (5 Å).

An ab initio simulated annealing protocol (Nilges et al., 1988a), starting from the template structure and using only unambiguous NOE distance constraints, was then applied to produce a set of 50 preliminary structures. NOE constraints were represented as "softsquare" potentials, i.e., as a square-well function within the allowed limits, and a soft asymptote outside these limits such that the energy increased linearly with the deviation from allowed limits. The simulated annealing protocol consisted of a short initial Powell minimization of the template structure (50 steps), followed by 20 ps of high-temperature molecular dynamics (Verlet dynamics at 1000 K, δt = 5 fs). At this stage, a dramatically reduced van der Waals potential is used (repel function, weight 0.002), and a low weighting on the NOE constraints is applied by selecting a low asymptote value. This was followed by 10 ps of dynamics at the same bath temperature with an increased weighting on local geometry and an increased weighting on the experimental NOE constraints. The system was then cooled to 100 K over 45 ps, with van der Waals repulsive potential terms gradually increased during the annealing phase. The structures were finally subjected to 500 cycles of Powell energy minimization. The ensuing examination of these 50 preliminary structures, obtained by ab initio simulated annealing, allowed many of the ambiguities in the assignment of NOE cross-peaks to be resolved. These structures suggested the existence of a potential disulfide bridge, involving the

cysteines residues 18 and 85. Lastly, the constraints based on paramagnetic broadening patterns were confirmed. After all possible constraints had been extracted, a new set of 100 structures were generated by the same ab initio simulated annealing protocol, from the NOE distance data. This protocol has been applied twice, i.e., 100 structures generated without imposing the Cys 18−Cys 85 disulfide bridge in the set of distance constraints and 100 structures generated with an imposed S−S covalent bond represented as a fake NOE distance (2.02 ± 0.1 Å). After elimination of clearly misfolded structures, the 100 structures, in each family, were further refined using a protocol similar to that of the first simulated annealing step (Nilges et al., 1988b). Hydrogen bonds for some of the slowly exchanging amide protons could also be identified and were added during the refinement steps. In the refinement procedure, the NOE constraints were represented as square-well potentials, with a constant weight throughout the protocol. Structures were initially heated to 1500 K and then cooled to 100 K for 45 ps (9000 steps, δt = 5 fs), while van der Waals repulsive terms (repel function) were gradually increased. Final refinement was achieved by restrained Powell energy minimization (200 steps) using the standard force field and parameter sets of X-PLOR. Resulting refined structures were analyzed for the best fit to the NMR constraints, and the overall energy. Two iterations of the refinement protocol were sufficient to generate nine and seven acceptable structures in each family (with and without an imposed disulfide bridge, respectively), as determined by the strict absence of NOE violations greater than 0.5 Å, or of torsion angle constraint violations greater than 5°. To study the secondary structure elements (see structure calculation results), only the violations occurring in these secondary structure elements were taken in account. However, structures which have violations larger than 1 Å (for the distance constraints) and 10° (for the dihedral angle constraints) in the other parts of the protein were eliminated. Geometric analysis of the refined structures was performed within X-PLOR (average structure computation and derivation of rmsd per residue). Structure visualization and superimpositions were accomplished using the SYBYL software package, version 6.1.

RESULTS AND DISCUSSION

Assignment

Sequence-specific assignment was achieved following the method devised by Wüthrich (1986). Spin systems of different amino acids were identified by their characteristic chemical shift pattern (Figure 1). Nevertheless, all the spin systems expected from *Syn.* 6803 Fd were not fully observed. Coupling of electronic and nuclear spins gives rise to "hyperfine" shifted resonances and to rapid nuclear relaxation leading to severe broadening of the resonances of the residues surrounding the paramagnetic iron−sulfur cluster. Oh and Markley (1990a) reported that the resonances of protons closer than 7.8 Å to both iron atoms in the oxidized form of *Anabaena* 7120 Fd were not observed in 2D proton spectra. In the case of *Syn.* 6803 Fd, we first performed ^{1}H TOCSY and NOESY homonuclear experiments. Analysis of these spectra led to assignment of only 66% of total residues and 83% of residues far from the cluster. Indeed, several residues either exhibited resonance degeneracy or were not detected in our ^{1}H spectra. In order to complete and confirm the preliminary assignment, uniformly ^{15}N-labeled Fd samples were prepared and 2D heteronuclear experiments spectra were acquired. With these samples, most of the residues far from the paramagnetic cluster were observed and assigned.

Side Chain Spin Systems. Sixty-three backbone amide resonances were correlated to side-chain spin systems by TOCSY (Figure 1) and COSY, recorded in H_2O and D_2O. All the resonances of the Tyr, Thr, Glu, and Cys residues, which are sufficiently far from the [2Fe-2S] cluster (distance larger than 8 Å), were assigned using homonuclear spectra. The Cys 18 and 85, which are not ligated to the [2Fe-2S] cluster, exhibit particular side chain chemical shifts. For each cysteine, the $H_{\beta 1}$ and $H_{\beta 2}$ resonances are strongly magnetically inequivalent (2.2/3.1 ppm and 2.4/3.2 ppm for the Cys 18 and 85, respectively). The aromatic spin systems of Tyr 3, 73, 80, and 96 were identified by intraresidue NOE cross-peaks observed between $^1H_\beta$, $^1H_\alpha$, NH, and aromatic resonances. The aromatic spin systems of Tyr 23 and 37 and of Phe 63 were not observed.

Overlaps in the aliphatic region of the COSY spectra interfered with tracing of scalar coupling connectivities for several residues, at different temperatures (20, 32, 37 °C), different pH values (5.0−7.0), and in the absence or the presence of salt (100 mM NaCl). This problem was partially solved using ^{1}H−^{15}N SQC-TOCSY and SQC-NOESY spectra obtained in either H_2O or D_2O, under the same conditions. The spin systems of three pairs of residues were always overlapping in the TOCSY spectra whatever the temperature or pH were: Leu 7 and Leu 16, Ile 69 and Thr 22, and Lys 6 and His 90 (Figure 1). They were resolved and assigned in the heteronuclear spectra, but the side chain chemical shifts of these residues were only partially determined.

^{1}H−^{15}N heteronuclear 2D NMR experiments allowed the resolution of 12 additional resonances (Figure 2). Asp 11, Asp 21, Leu 25, Gly 49, Ser 59, Gln 61, Leu 64, Asp 67, Val 74, Ala 79, Ser 83, and Asp 84 were only observed on ^{1}H−^{15}N SQC spectra and then assigned using sequential cross-peaks on SQC-NOESY spectra. Cross-peaks determined on heteronuclear TOCSY spectra corresponded to Asp 11, Leu 25, Ser 59, Val 74, and Ala 79 and were then identified in ^{1}H-^{1}H NOESY spectra. The $^{15}NH_2\gamma$ resonances of the glutamine residues 58, 61, and 68 were identified on heteronuclear spectra (Figure 2). ($^{15}NH_2\gamma$)Gln 58 has been assigned by intraresidue cross-peaks between $^{15}NH_2\gamma$ and H_α on one side and Hβ on the other side on SQC-NOESY spectra. ($^{15}NH_2\gamma$)Gln 68 was identified by interresidue connectivities between Glu 67 and Gln 68. As a consequence, the last two connectivities in SQC spectra, characteristic of a ($^{15}NH_2\gamma$)Gln, that have no intra- or interresidue connectivity, were attributed to ($^{15}NH_2\gamma$)Gln 61.

Broadened Cross-Peaks. In ^{1}H−^{15}N spectra, several peaks were broadened (Figure 2, square boxes), and the corresponding peaks in the homonuclear TOCSY spectra were not observed. Nevertheless, for some of them (Leu 25, Leu 35, Ser 62, Val 74, and Ala 79), NOE cross-peaks found in the homonuclear spectra allowed their assignment. The spin system of Arg 40 was partially observed on ^{1}H−^{15}N spectra. Only the N_ϵ of Arg 40 was observed in SQC spectra (Figure 2). This cross-peak ($^{15}N_\epsilon$−^{1}H) is broadened and shifted because of the proximity of the paramagnetic cluster. It was observed in the SQC-TOCSY or SQC-NOESY spectra.

Resonances and spin-systems from 76 residues were observed and identified on homo and heteronuclear TOCSY and NOESY spectra. Resonances from 20 residues sur-

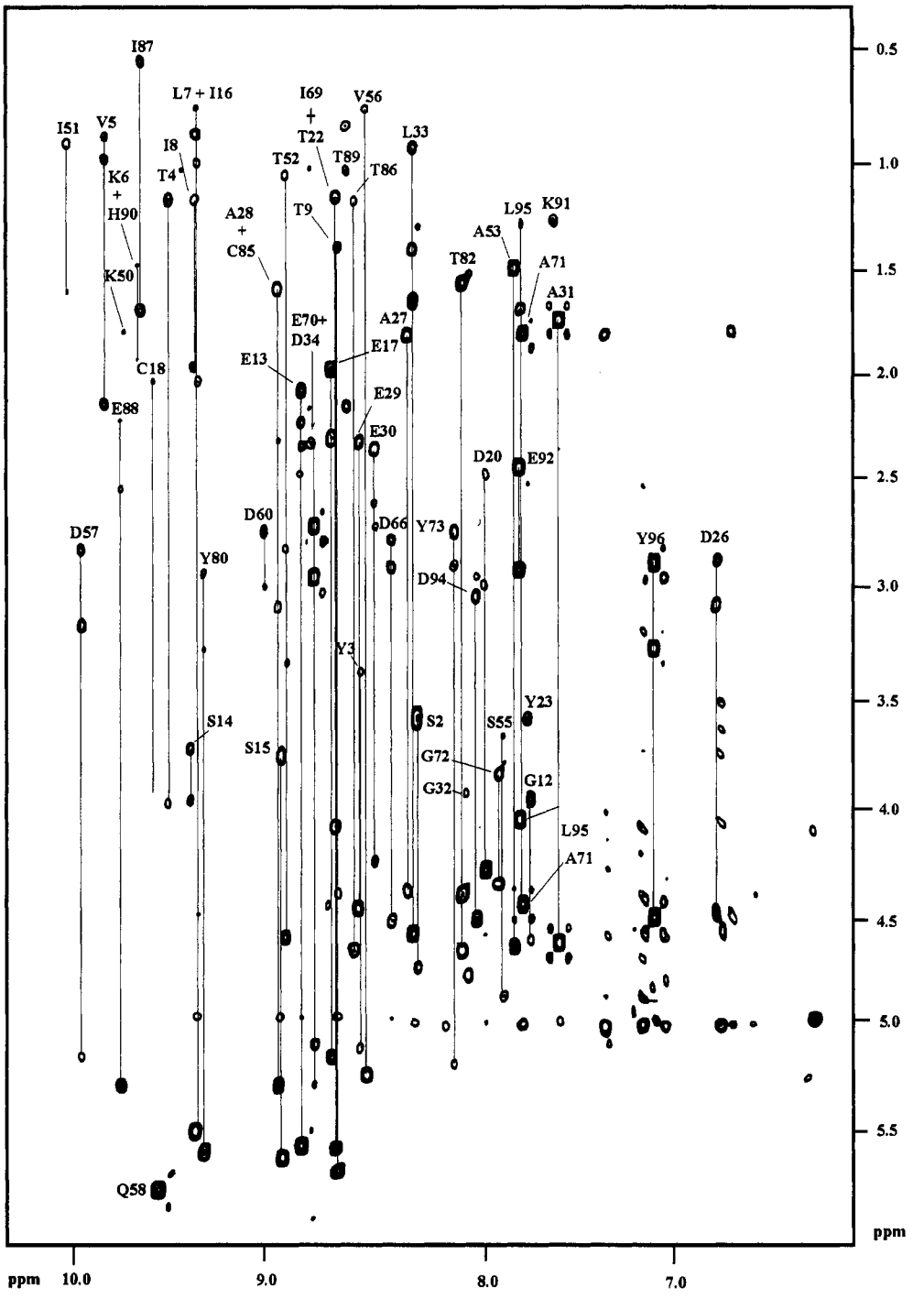

FIGURE 1: Portion of the 600 MHz ^{1}H-TOCSY spectrum of oxidized Fd (τ_m = 80 ms). The sample consisted of 0.5 mL of 5−8 mM Fd in (90:10) H_2O/D_2O containing 100 mM NaCl, 100 mM phosphate buffer at pH 5.0.

rounding the iron−sulfur cluster were not observed on 2D spectra. Residues that have not been detected are the (Pro 36−Ala 48) and (Leu 75−Val 78) segments and the Phe 63, Ile 24, and Pro 81 residues. A list of ^{1}H and ^{15}N resonance assignment for oxidized Fd (100 mM NaCl, 100 mM phosphate buffer at pH 5.0, 20 °C) is given in Table 3 of the Supporting Information.

Secondary Structure

Identification of α Helix and β Sheet. Figure 3 shows observed sequential (i,i+1) to (i,i+4) NOE connectivities. Weak or medium αN (i,i+1), strong or medium NN(i,i+1), and weak or very weak (i,i+2) and (i,i+3) connectivities characteristic of an α helix were observed for three segments (Wüthrich et al., 1983): Asp 26−Asp 34, Asp 66−Glu 70, and Glu 93−Tyr 96 (Figure 3). The Hα chemical shift of these residues also exhibits an upfield shift (Figure 4), with respect to the random coil values (Merutka et al., 1995). This is characteristic of an α helix (Wishart et al., 1991).

Three regions display characteristic sequential β strand connectivities (Wüthrich et al., 1983): strong and medium αN(i,i+1) and weak NN(i,i+1) (Figure 3). Figure 5 shows the long-range NOE connectivities which are characteristic of a β sheet composed of four β strands. They were designated A, B, C, and D strands. A and B strands are antiparallel as are C and D. C and B strands are parallel. The clearly identified NOE connectivities between the β strands A and B, between B and C and between C and D are shown in Figures 5 and 6. Figure 4 shows that Hα

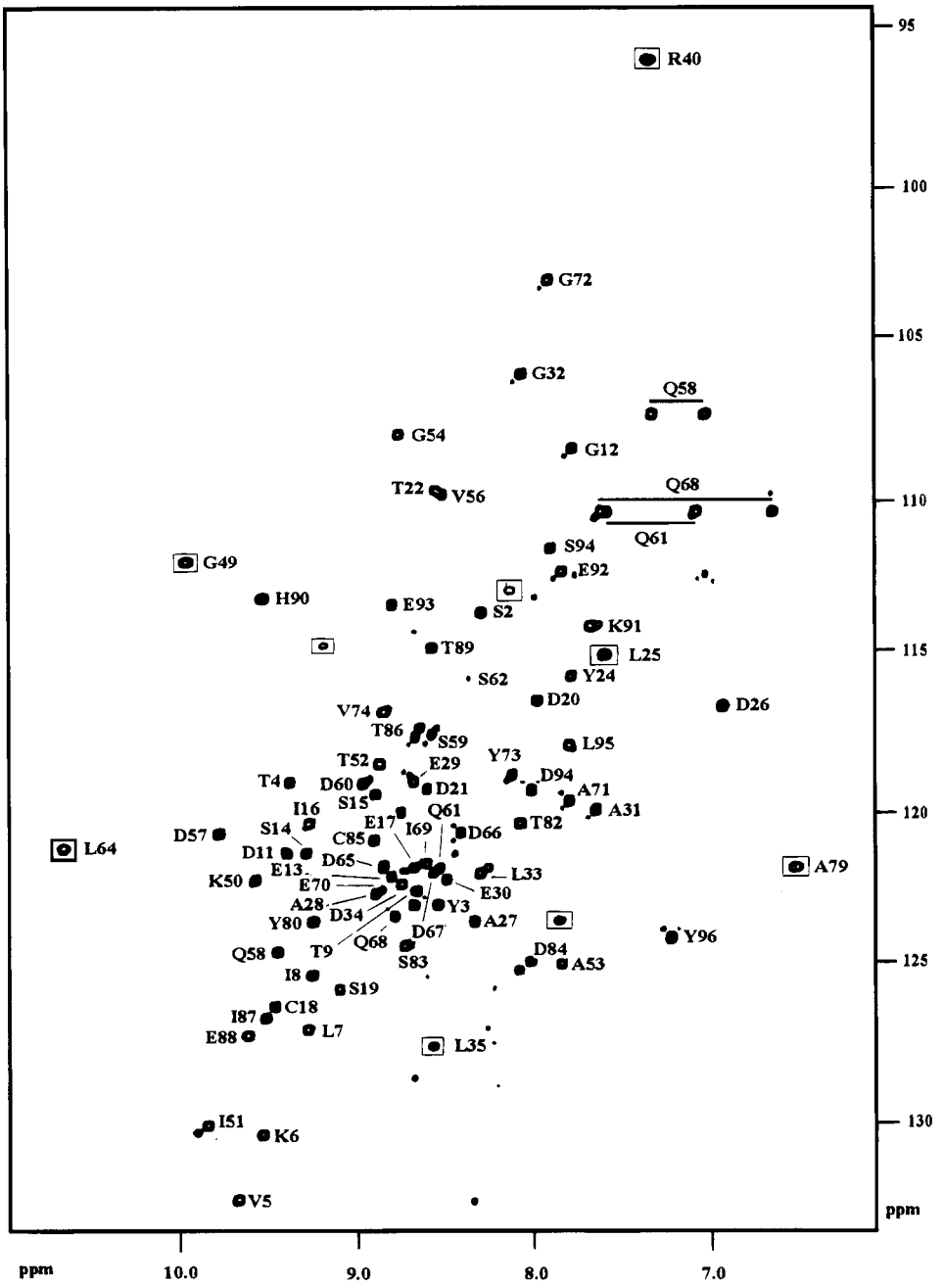

FIGURE 2: $^1H[^{15}N]$ HSQC spectrum (500 MHz ^1H, 50 MHz ^{15}N) of oxidized ferredoxin. The protein concentration was 8 mM. Samples were in (90:10) H_2O/D_2O 100 mM phosphate buffer, and 100 mM NaCl, pH 6.5. The temperature was 20 °C. The square boxes indicate the broadened cross-peaks which disappear on SQC-NOESY and SQC-TOCSY spectra.

resonances of residues located in the Ala 1−Thr 9, Gly 12−Ser 19, Gly 49−Ser 55, and Thr 82−His 90 segments are systematically shifted downfield [with respect to the random coil values (Merutka et al., 1995)]. As observed in Figure 6, one can notice the observed NOEs were not consistent with a planar β sheet (dashed arrows). The N-terminal part of the β (B) strand does not seem to be included in the β sheet because of the apparent proximity of the A and C β strands in this region. The A and C β strands seem to be closer in *Syn.* 6803 Fd than in the homologous Fd structure from *A. sacrum* or *A. variabilis*. In addition, some NOEs detected between the C and D β strands are not consistent with a planar β sheet. The NOE connectivities inconsistent with a planar β sheet involve the Cys 85, Glu 17, and Cys 18 residues.

H−D Exchange and T_2 Measurements. H−D exchange measurements show that 45 from 84 observable amide protons and NH_2 side chain protons were not exchanged after 4 days in D_2O (Figure 3). Chae et al. (1994) have observed that, after 30 h, 35 of 80 (= 44%) and 23 of 75 (= 31%) observable amide protons from vegetative and heterocyst Fd, respectively, were not exchanged. By contrast, the proportion of slowly exchangeable protons in *Syn.* 6803 Fd is significantly higher than in vegetative or heterocyst Fds from *Anabaena*. This difference could be explained by the formation of a Fd dimer in *Syn.* 6803, even if there were no experimental NOE observed consistent with such an oligomerization.

We performed ^{15}N T_2 measurements on non exchangeable NH amide groups in ^2H_2O (using 2D heteronuclear correlation experiments at 20 °C). The average T_2 value was found to be 118 ms. This value can be compared to those measured for proteins having a similar molecular mass as *Syn.* 6803 Fd: immunophiline, Cter domain of the phospholipase SH2,

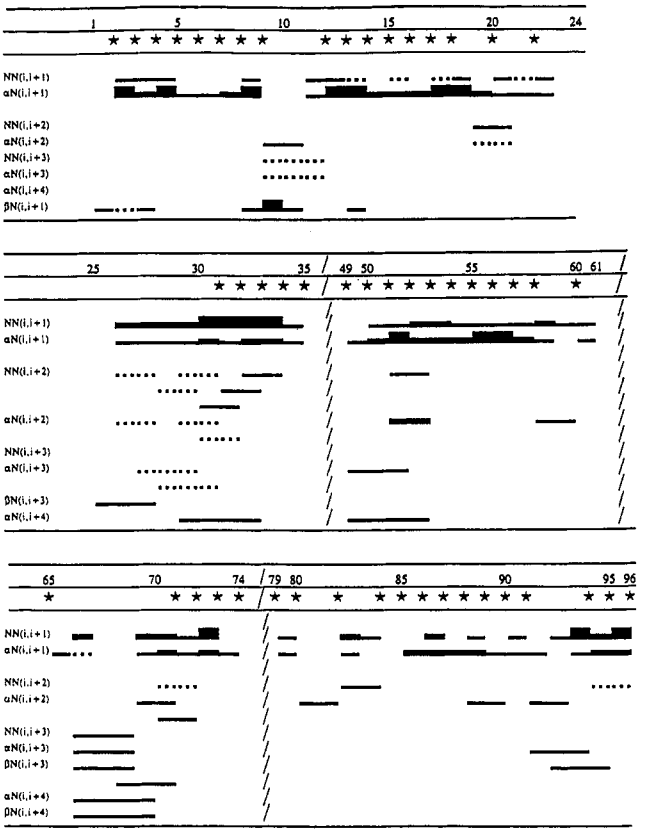

FIGURE 3: Sequential NOE connectivities used to identify secondary structure elements in [2Fe-2S] Ed from *Syn.* 6803 and used as constraints in the structural calculations. The thicker lines represent strong NOEs, the medium lines, medium NOEs, the thin lines, weak NOEs and the dashed lines, very weak NOEs. The (/) symbols indicate amino acid residues for which no sequential NOEs were observed. The stars represent the residues the amide proton of which is not exchanged in D_2O after 4 days, as defined by the observation of a cross-peak in $^1H-^{15}N$ SQC spectra.

thioredoxin, and the V_L domain of antibody are composed of 107, 105, 108, and 113 amino acid residues, respectively (Cheng et al., 1994; Farrow et al., 1994; Stone et al., 1993; Constantine et al., 1993). The average T_2 values of these proteins, measured at 30 or 35 °C, range from 85 to 115 ms. Therefore, the T_2 measurement of *Syn.* 6803 Fd performed at 20 °C indicates that the protein is monomeric. T_2 and H−D exchange measurements suggest that the *Syn.* 6803 Fd exhibits a higher conformational stability from that of the other chloroplast-type Fds.

The *Syn.* 6803 Fd shows also some chemical and physical features different from the other chloroplast-type Fds. Bottin and Lagoutte (1992) have observed that the *Syn.* 6803 Fd has an unusual electrophoretic migration compared to that of spinach Fd. The apparent molecular mass of *Syn.* 6803 Fd is dependent on the electrophoretic conditions: the apparent M_r varies from 2.5 (native) to 16.5 kDa (reduced). An intermediate low value of 3.5 kDa is found after incubation of the Fd in urea. The presence of a disulfide bridge in *Syn.* 6803 Fd was hypothesized since the nonreduced form of a protein containing a disulfide bridge would exhibit a greater mobility. Indeed, the disulfide bridge restricts the flexibility of the unfolded polypeptide chain and decreases its hydrodynamic volume (Creighton, 1989). Bottin and Lagoutte (1992) have also performed free thiol assays with native and denatured *Syn.* 6803 Fd. Under both conditions, the reaction was negative whereas with spinach Fd, one free thiol group per protein molecule was detected.

The observed NOEs (around Cys 18 and 85) together with the unusual electrophoretic pattern and the high conformational stability of *Syn.* 6803 Fd could suggest the existence of a disulfide bridge between Cys 85 and Cys 18. This disulfide bridge could also explain the high chemical shift difference (around 1 ppm) observed between the $H_{\beta 1}$ and $H_{\beta 2}$ of each of the cysteine residues.

Structure Calculation Results

Main Features of Syn. 6803 Fd Structure Models. Structural calculations, using the X-PLOR program, were performed to determine the three-dimensional structure of *Syn.* 6803 Fd. A total of 831 distance constraints is not sufficient to define a well resolved structure but allows to determine the tertiary fold. The lack of constraints is essentially due to the paramagnetic effect of the [2Fe-2S] cluster which affects all the surrounding residues. As a result, the majority of the constraints involve residues which are far from the iron−sulfur cluster and present in secondary structure elements. Therefore, these segments will be better defined than the segments surrounding the [2Fe-2S] cluster. To model the *Syn.* 6803 Fd structure, two types of calculations were performed. In one case, a disulfide bridge was imposed during all the calculations, and, in another case, no disulfide bridge has been imposed. Two families of structures, respectively named "DB" and "no DB", were derived.

Both families ("DB" and "no DB") exhibited the same tertiary fold (Figure 7). Secondary structure elements, an α helix, two α helix turns, and a β sheet, described above, were observed. In both families, the rms deviation is high, close to 2.2 Å. Figure 8 shows that high rms deviations and low NOE constraints are correlated. As a consequence it was not possible to superimpose all the structures of a family in a single diagram. To circumvent this problem, we decomposed the structure into several elements corresponding to regions of smaller rms deviations and higher rms deviations. Taken separately, all the segments comprising the secondary structure elements (β sheet

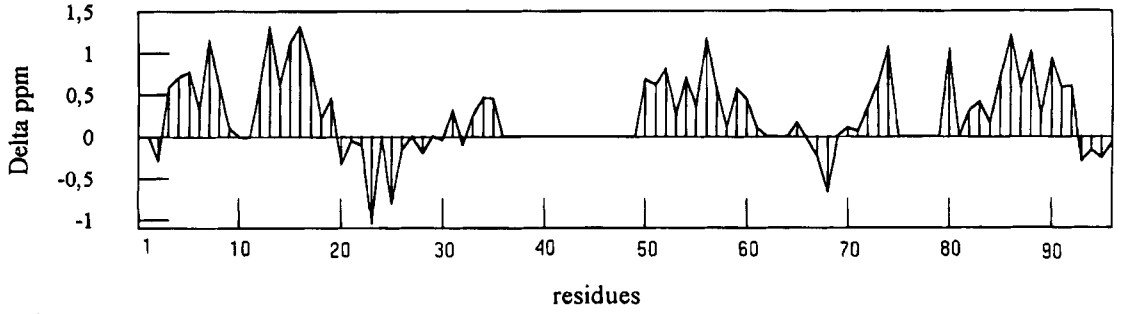

FIGURE 4: Difference between the observed chemical shift Hα of each residue (ppm) and the corresponding random coil value (Merutka et al., 1995).

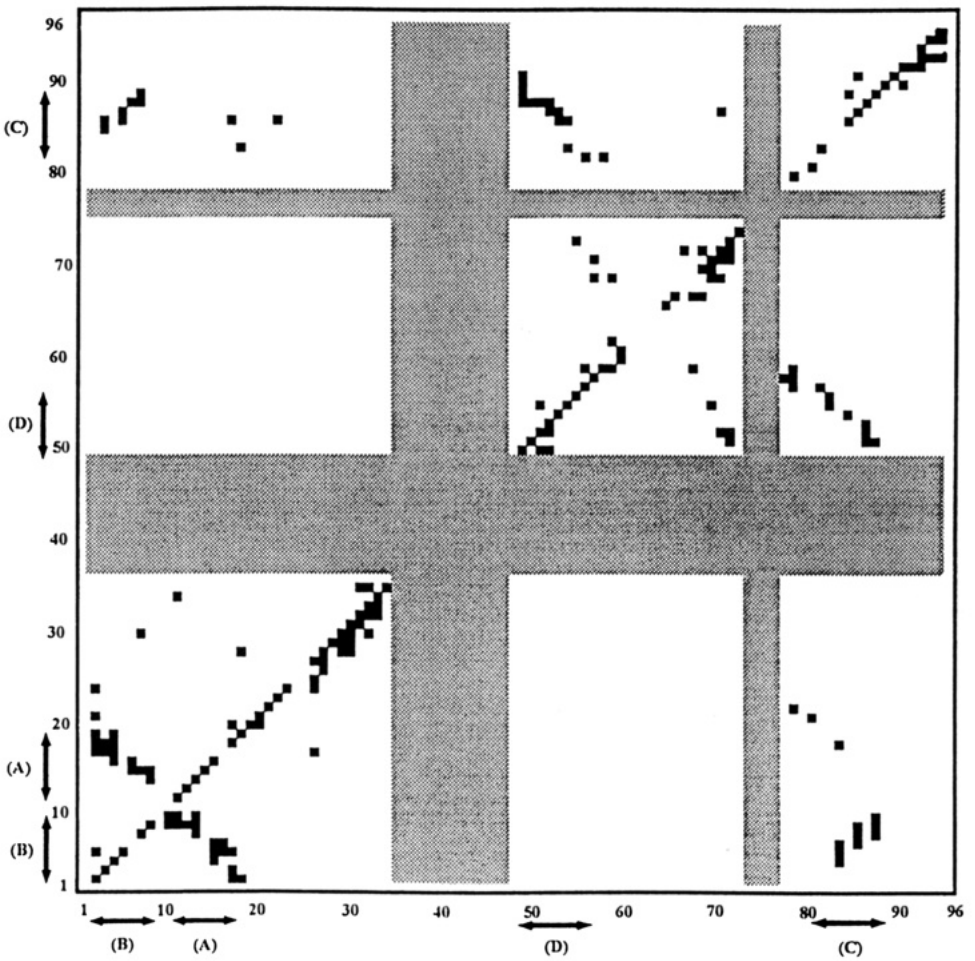

FIGURE 5: Interresidue NOEs identified in *Syn.* 6803 Fd and used as constraints for structural calculations. One square is generated for each pair of residue *i* and *j* which were connected by NOE connectivities. A, B, C, and D correspond to the β strands described in Figure 6. The dashed areas correspond to amino acid residues surrounding the paramagnetic cluster.

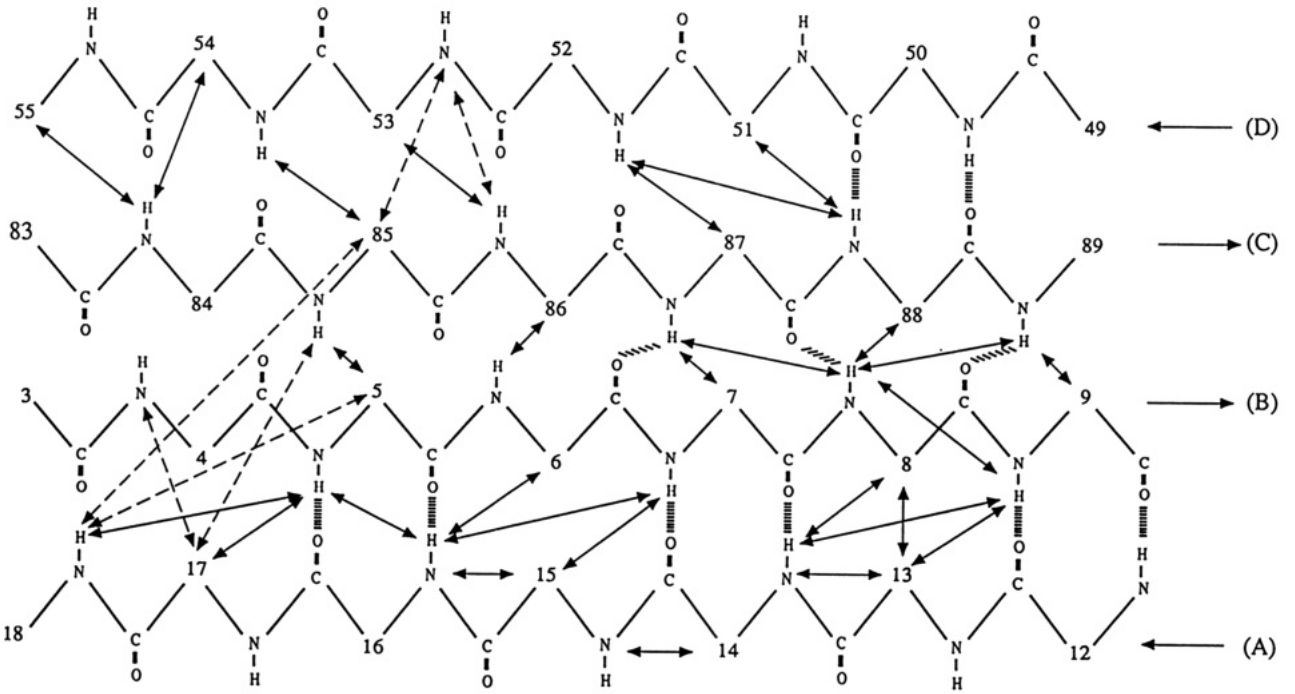

FIGURE 6: β Sheet identified by intra- and interresidue NOEs (solid arrows). Dashed arrows show the observed interresidue NOEs inconsistent with a planar β sheet structure. Broken lines represent hydrogen bonds (identified by amide protons still present after 4 days in D_2O phosphate buffer) used for structural simulations.

and α helices) were well defined. In contrast, the segments linking these secondary structure elements were not well defined.

Segments with the Higher rms Deviations. Figure 8a shows that the highest rms deviations values are found for the segments: Ala 31−Ala 48, Gln 61−Asp 67, Tyr 73−

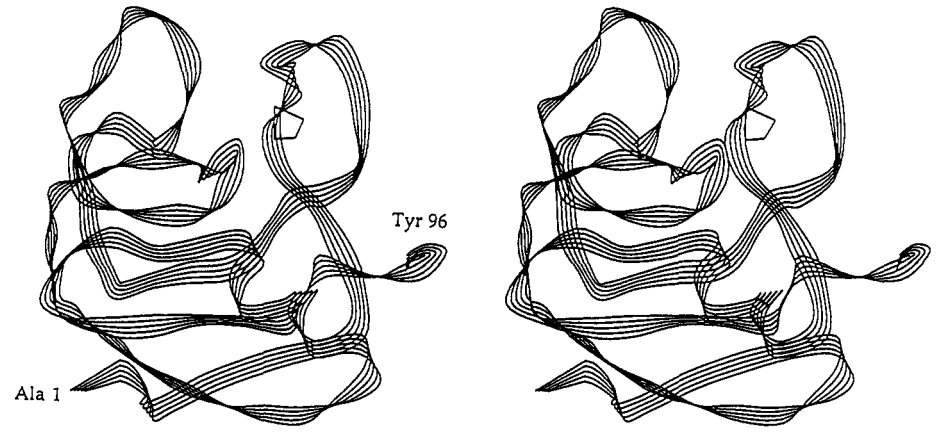

FIGURE 7: Stereodiagram of one of the "DB" (including a disulfide bridge) acceptable structure of lowest energy.

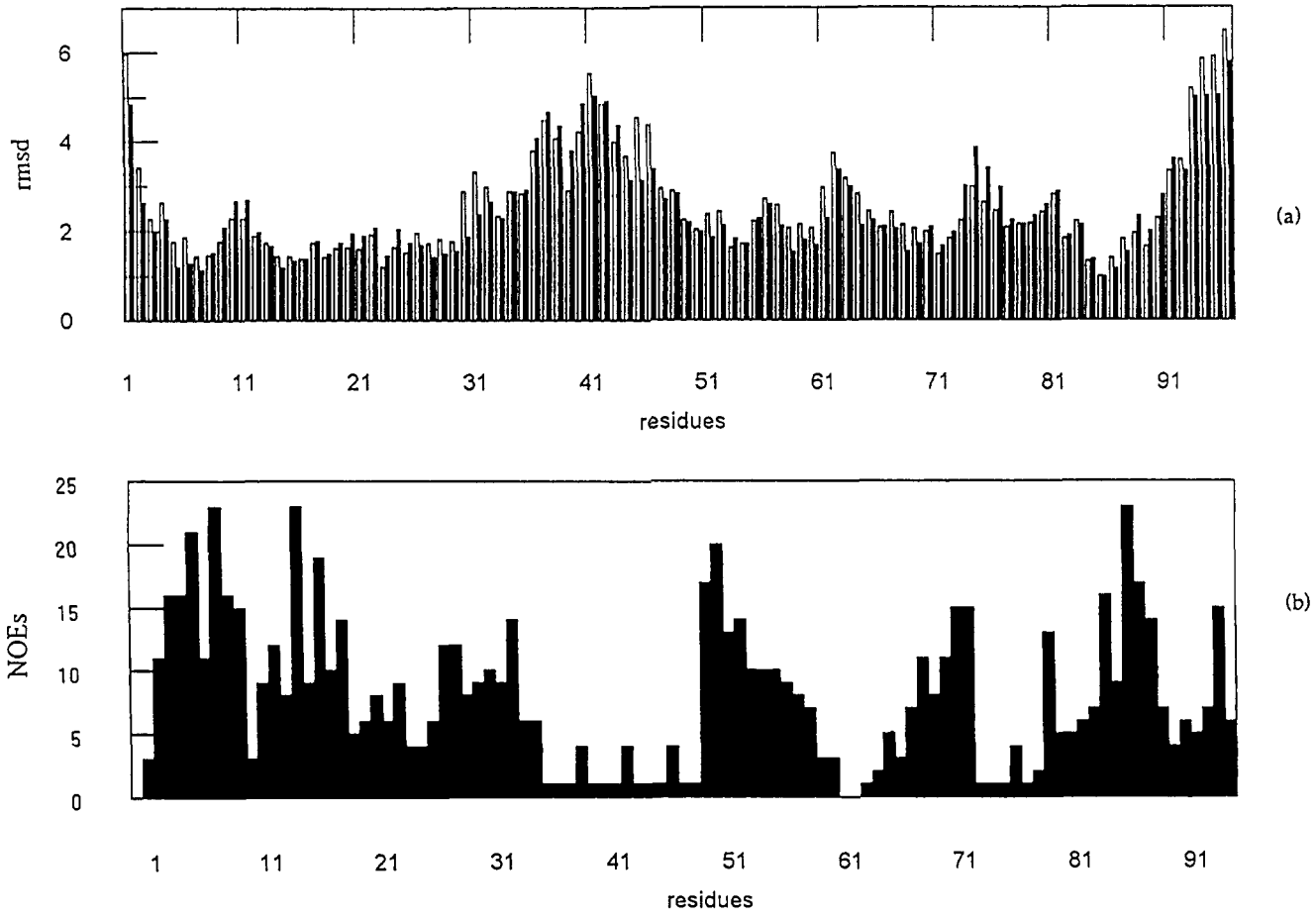

FIGURE 8: (a) Rms deviations for the backbone of each family. The family structure generated by X-PLOR including a disulfide bridge is shown in black. The family structure generated by X-PLOR with no imposed disulfide bridge is shown in gray. (b) Number of interresidue NOE constraints per residue used in the calculations.

Ser 83 and N and C termini. In a given family, for any of these segments, the structures were not superimposable. This variability is due to the lack of NOE constraints between the corresponding residues and the remaining part of the protein. As already mentioned, the high rms deviations correlate with a lower number of NOE constraints used in the calculations (Figure 8b). This deficit of NOEs has two origins. First, some residues of the protein are exposed to the solvent and very flexible, with no or few contacts with the nearest residues: this is the case for the C terminus (His90−Tyr 96), the N terminus (Ala 1−Ser 2), and the Gln 61−Asp 67 segment. Paramagnetic effects also decrease the number of long range interresidues NOE constraints (Bertini et al., 1993). The Pro 36−Ala 48 and Leu 75−Val 78 segments and the Ile 24 and Phe 63 residues were not observed on 2D spectra. The Leu 25, Leu 35, Gly 49, Leu 64, and Ala 79 residues exhibit broadened resonances and are only observed on heteronuclear spectra (Figure 2). As a result, few connectivities were observed around Ile 24−Leu 25, Asp 34−Leu 35, Gly 49−Lys 50, Leu 64−Asp 65, and Ala 79−Tyr 80 segments (Figure 8b). In order to model the environment of the [2Fe-2S] cluster, constraints based on bond lengths and dihedral angles measured in *A. sacrum* [2Fe-2S] Fd X-ray structure were used as NOE constraints (see Materials and Methods). However, these constraints were not sufficient to generate a well defined structure for these parts of *Syn.* 6803 Fd.

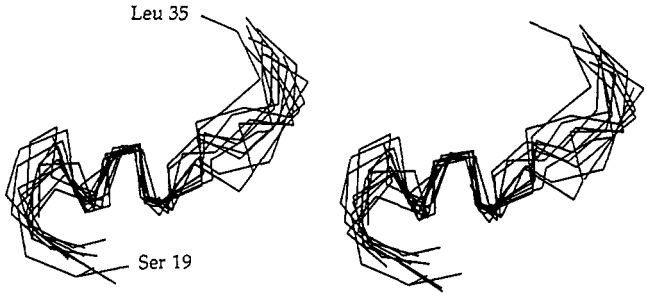

FIGURE 9: Superimposition of the segment (Ser 19−Leu 35) including the α helix of all acceptable structures generated with and without disulfide bridge.

Segments with the Smaller rms Deviations. In both families ("DB" and "no DB" family), the well defined segments are composed of the secondary structure elements (β sheet and α helices). All secondary structure elements deduced from the NOE data (Figures 3, 5 and 6) are confirmed by the calculations. A β sheet composed of four β strands, one α helix (Tyr 23−Leu 33), and two α helix turns (Asp 66−Glu 70 and Glu 93−Tyr 96) are observed in both families.

The α Helices. The two α helix turns Asp 66−Glu 70 and Glu 93−Tyr 96 are well superimposable (data not shown). Figure 9 shows the superimposition of the α helix

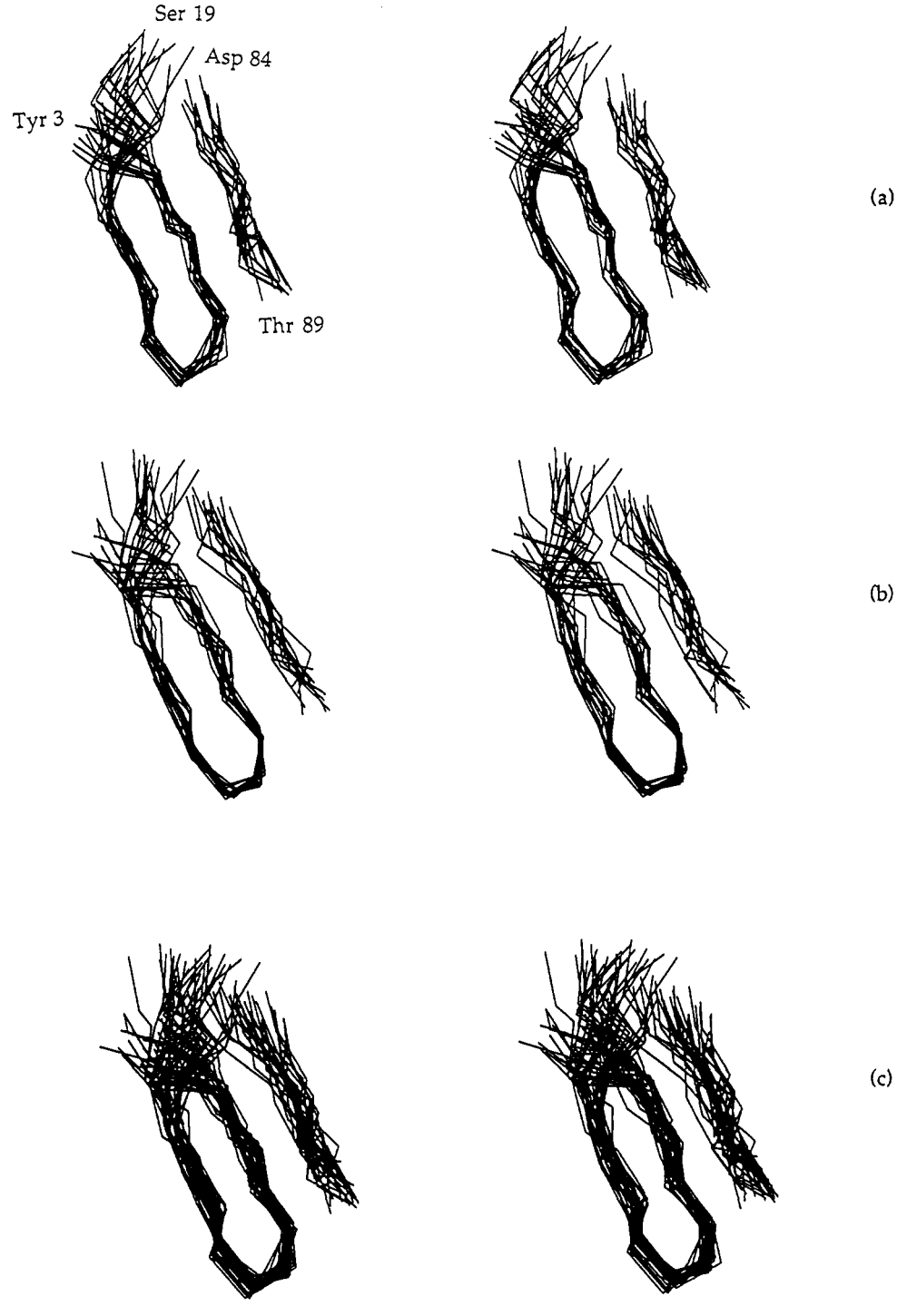

FIGURE 10: Superimposition of a part of the β sheet (Tyr 3−Ser 19 and Asp 84−Thr 89 segments) from the accepted structures generated by calculations (a) not including a disulfide bridge and (b) including a disulfide bridge. Part c displays the superimposition of parts a and b.

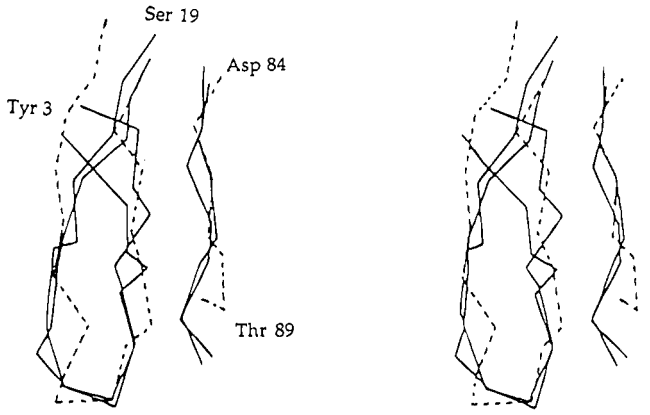

FIGURE 11: Superimposition of the β sheet structures (Tyr 3−Ser 19) and (Asp 84−Thr 89) segments from three Fd structures: two calculated structures belonging to the "no DB" family are superimposed. One of them correspond to the "up" and the other one to the "down" structure (see text). The β sheet structure of *A. sacrum* Fd is represented in dashed line.

Tyr 23−Leu 33 extracted from all acceptable structures of each family ("DB" + "no DB"). The α helices (Tyr 23−Leu 33) are not well superimposable on their whole length (Figure 9), because of the lack of NOE constraints at the extremities (Ile 24−Leu 25 and Asp 34−Leu 35).

The β Sheet. Figure 10 shows the superimposition of the most part of the β sheet (A, B, and C β strands) from 15 calculated structures in each family ("DB" and "no DB"). These 30 calculated structures show no NOE violations larger than 0.5 Å. In some of them, dihedral constraint violations larger than 5° have been observed, but none of these violations are found in the β sheet. The D β strands from the different structures (not shown in Figure 10) are not well superimposable. This is most likely due to the few numbers of observed NOE constraints between the C and D β strands (Figure 6). In both families ("DB" and "no DB"), two substructures were observed. They differ by the position of the N terminal segment (Ala 1−Thr 4) with respect to the β sheet plane (Figure 11): the N-terminal part of the B β strand crossed the A β strand under the β sheet plane in one case and above the plane in the other case. One cannot distinguish between these two solutions on the basis of the NOE data. The corresponding substructures are designated "up" or "down" for "DB" or "no DB".

The Disulfide Bridge. The β sheets of both families ("DB" and "no DB") were superimposable (Figure 10c). As described previously, the N and C termini are very flexible. Figure 11 shows the superimposition of the β sheets from *A. sacrum* Fd and from each subfamily ("up" and "down") of the "no DB" family. In the case of the β sheet from *A. sacrum* Fd, the three β strands (A, B, and C) are planar. In both subfamilies ("up" and "down") calculated with no imposed disulfide bridge, the end of the A β strand crosses the B β strand. As a consequence, the extremity of the A β strand is close to the C β strand. The distance between the sulfur atoms of Cys 18 and Cys 85 was measured on each model structure of the "no DB" family. It ranges between 3.74 and 11.05 Å with an average of 7.32 Å. Although this average distance is quite large for most of obtained structures, a small rotation about the $C_\alpha-C_\beta$ bond of cysteine residues would bring the two sulfur atoms sufficiently close to form a disulfide bridge.

Comparison with Homologous [2Fe-2S] Fd X-ray Structures

The tertiary fold of *Syn.* 6803 [2Fe-2S] Fd (Figure 7) shows the same structural arrangement as that of the chloroplast-type Fd extracted from *Spirulina platensis*, *A. sacrum*, or *Anabaena* 7120 determined by X-ray crystallography. In particular, the main secondary structure element is a four-stranded β sheet. An α helix (Tyr 23−Leu 33 for *Syn.* 6803 Fd) is also found in all homologous chloroplast-type Fds. As first hypothesized by Pochapsky et al. (1994), it has been assumed that the structure of the [2Fe-2S] cluster and its surroundings is structurally invariant in all types of [2Fe-2S] Fds. For modeling *Syn.* 6803 Fd, the distances measured on a X-ray Fd structure have been used to stabilize the backbone in a conformation consistent with the observed NOE data. However, this was not sufficient to obtain low rms deviations for the segments surrounding the paramagnetic cluster. The major difference between *Syn.* 6803 Fd and the other chloroplast-type Fd structures is the probable presence of a disulfide bridge between Cys 18 and Cys 85. Such a disulfide bridge has never been described in chloroplast-type Fd containing six cysteine residues. This disulfide bridge could be responsible for the distortions in one extremity of the β sheet. The A and C β strands containing the cysteine residues (Figure 6) are closer in the present model of *Syn.* 6803 Fd than in the structure from *Spirulina platensis* or *Anabaena* 7120 Fds. The 3D structure determined by X-ray crystallography of a Fd that contains six cysteine residues (Tsukihara et al., 1981) shows that this protein contains also two free cysteine residues included in a β sheet. In the crystal the two thiol groups are too far (approximately 10 Å) to be involved in a disulfide bridge.

The present study proposes a tertiary fold of *Syn.* 6803 Fd which is slightly different from the tertiary fold of homologous ferredoxins determined by X-ray studies. The structural arrangement of *Syn.* 6803 Fd suggests the presence of a disulfide bridge between Cys 18 and Cys 85. The existence of this disulfide bridge must be confirmed. To complete these structural studies, specific labeling of cysteine residues or directed mutagenesis of *Syn.* 6803 Fd would provide useful information. The specific labeling of the cysteine residues would also allow the study of the environment of the paramagnetic cluster in a Fd purified from a vegetative cell. Such data could then be compared to the results already obtained for the heterocyst *Anabaena* Fd (Chae & Markley, 1995), in order to understand the structural differences observed between the Fds extracted from heterocyst and vegetative cells (Chae et al., 1994). Our results provide the first step in studying the interaction of the *Syn.* 6803 Fd with the different ferredoxin-dependent proteins.

ACKNOWLEDGMENT

We thank Dr. Alain Sanson for stimulating discussions and careful reading of the manuscript. We also thank Dr. Sun Un for careful reading of the manuscript.

SUPPORTING INFORMATION AVAILABLE

Three tables giving the distances and dihedral angles between the ligating cysteines and the cluster used for generating the "initial structure", distance and dihedral angle constraints used for modeling the cluster and its surroundings

the structural calculations, and ^{1}H and ^{15}N resonance assignment for oxidized [2Fe-2S] Fd in 100 mM NaCl, 100 mM phosphate buffer at pH 5.0, 20 °C (5 pages). Ordering information is given on any current masthead page.

REFERENCES

Bertini, I., Turano, P., & Vila, A. J. (1993) *Chem. Rev. 93*, 2833−2932.

Bottin, H., & Lagoutte, B. (1992) *Biochim. Biophys. Acta 1101*, 48−56.

Brünger, A. T. (1992) X-PLOR 3.0 version, Yale University Press, New Haven, CT.

Chae, Y. K., & Markley, J. L. (1995) *Biochemistry 34*, 188−193.

Chae, Y. K., Abildgaard, F., Moobery, E. S., & Markley, J. L. (1994) *Biochemistry 33*, 3287−3295.

Chan, T.-M., & Markley, J. L. (1983a) *Biochemistry 22*, 5982−5987.

Chan, T.-M., & Markley, J. L. (1983b) *Biochemistry 22*, 5988−5995.

Chan, T.-M., & Markley, J. L. (1983c) *Biochemistry 22*, 5996−6002.

Chan, T.-M., & Markley, J. L. (1983d) *Biochemistry 22*, 6002−6007.

Chan, T.-M., & Markley, J. L. (1983e) *Biochemistry 22*, 6008−6010.

Cheng, J. M., Lepre, C. A., & Moore, J. M. (1994) *Biochemistry 33*, 4093−4100.

Constantine, K. L., Friedrichs, M. S., Goldfarb, V., Jeffrey, P. D., Sheriff, S., & Mueller, L. (1993) *Proteins: Struct., Funct. Genet. 15*, 290−311.

Creighton, T. E. (1989) in *Protein Structure*, pp 155−167, IRL Press, Oxford University Press, Oxford, U.K.

Dugad, L. B., La Mar, G. N., Banci, L., & Bertini, L. (1990) *Biochemistry 29*, 2263−2271.

Farrow, N. A., Muhandiram, R., Singer, A. U., Pascal, S. M., Kay, C. M., Gish, G., Shoelson, S. E., Pawson, T., Forman-Kay, J. D., & Kay, L. E. (1994) *Biochemistry 33*, 5984−6004.

Gronenborn, A. M., Bax, A., Wingfield, P. T., & Clore, G. M. (1989) *FEBS Lett. 243*, 93−98.

Ho, K.-K., Ulrich, E. L., Krogmann, D. W., & Gomez-Lojero, C. (1979) *Biochim. Biophys. Acta 545*, 236−248.

Ikemizu, S., Bando, M., Sato, T., Morimoto, Y., & Tsukihara, T. (1994) *Acta Crystallogr. D50*, 167−174.

Jacobson, B. L., Chae, Y. K., Markley, J. L., Rayment, I., & Holden, H. M. (1993) *Biochemistry 32*, 6788−6793.

Kay, L. E., Torchia, D. A., & Bax, A. (1989) *Biochemistry 28*, 8972−8979.

Knaff, D. B., & Hirasawa, M. (1991) *Biochim. Biophys. Acta 1056*, 93−125.

Lerner, L., & Bax, A. (1986) *J. Magn. Reson. 69*, 375−385.

Matsubara, H., & Wada, K. (1988) *Methods Enzymol. 167*, 387−410.

Matsubara, H., & Saeki, K. (1992) *Adv. Inorg. Chem. 38*, 223−280.

Merutka G., Dyson, H. J., & Wright P. E. (1995) *J. Biomol. NMR 5*, 14−24.

Nagayama, K., Ozaki, Y., Kyogoku, Y., Hase, T., & Matsubara, H. (1983) *J. Biochem. (Tokyo) 94*, 893−902.

Nilges, M., Gronenborn, A. M., & Clore, G. M. (1988a) *FEBS Lett. 239*, 129−136.

Nilges, M., Gronenborn, A., Brünger, A. T., & Clore, G. M. (1988b) *Protein Eng. 2*, 27−38.

Oh, B.-H., & Markley J. L. (1990a) *Biochemistry 29*, 3993−4004.

Oh, B.-H., & Markley, J. L. (1990b) *Biochemistry 29*, 4012−4017.

Oh, B.-H., Moobery, E. S., & Markley, J. L. (1990) *Biochemistry 29*, 4004−4011.

Plateau, P., & Gueron, M. (1982) *J. Am. Chem. Soc. 104*, 7310−7311.

Pochapsky, T. C., & Ye, X. M. (1991) *Biochemistry 30*, 3850−3856.

Pochapsky, T. C., Ye, X. M., Ratnaswamy, G., & Lyons, T. A. (1994) *Biochemistry 33*, 6424−6432.

Poe, M., Phillips, W. D., Glickson, J. D., McDonald, C. C., & San Pietro, A. (1971) *Proc. Natl. Acad. Sci. U.S.A. 68*, 68−71.

Rippka, R., Déruelles, J., Waterbury, J. B., Herdman, M., & Stanier, R. Y. (1979) *J. Gen. Microbiol. 111*, 1−61.

Rogers, L. J. (1987) in *The Cyanobacteria* (Fay, P., & Van Baalen, C., Eds.) pp 35−67, Elsevier, Amsterdam.

Rypniewski, W. R., Breiter, M. M., Wesenberg, G., Oh, B.-H., Markley, J. L., Rayment, I., & Holden, H. M. (1991) *Biochemistry 30*, 4126−4131.

Salmeen, I., & Palmer, G. (1972) *Arch. Biochem. Biophys. 150*, 767−773.

Shaka, A. J., Barker, P. B., & Freeman, R. (1985) *J. Magn. Reson. 64*, 547−552.

Skjeldal, L., Westler, W. M., Oh, B.-H., Krezel, A. M., Holden, H. M., Jacobson, B. L., Rayment, I., & Markley, J. L. (1991) *Biochemistry 30*, 7363−7368.

Stone, M. J., Chandrasekar, K., Holmgen, A., Wright, P. E., & Dyson, H. J. (1993) *Biochemistry 32*, 426−435.

Tsukihara, T., Fukuyama, K., Nakamura, M., Katsube, Y., Tanaka, N., Kakudo, M., Wada, K., Hase, T., & Matsubara, H. (1981) *J. Biochem. (Tokyo) 90*, 1763−1773.

Tsukihara, T., Fukuyama, K., Mizushima, M., Harioka, T., Kusunoki, M., Katsube, Y., Hase, T., & Matsubara, H. (1990) *J. Mol. Biol. 216*, 399−410.

Wishart, D. S., Sykes, B. D., & Richards, F. M. (1991) *J. Mol. Biol. 222*, 311−333.

Wüthrich, K. (1986) *NMR of Proteins and Nucleic Acids*, John Wiley, New York.

Wüthrich, K., Billeter, M., & Braun, W. (1983) *J. Mol. Biol. 169*, 949−961.

Ye, X. M., Pochapsky, T. C., & Pochapsky, S. S. (1992) *Biochemistry 31*, 1961−1968.

BI9515580